

Simulation Models for Superconducting Components of the Electric Aircraft

Ali Khonya
Institute for Technical Physics
Karlsruhe Institute of Technology
Karlsruhe, Germany
Ali.khonya@kit.edu

Mathias Noe
Institute for Technical Physics
Karlsruhe Institute of Technology
Karlsruhe, Germany
Mathias.noe@kit.edu

Wescley Tiago Batista de Sousa
Institute for Technical Physics
Karlsruhe Institute of Technology
Karlsruhe, Germany
Sousa@kit.edu

Frederick Berg
Airbus X-labs
Taufkirchen, Germany
Frederick.berg@airbus.com

Michael Cooper
Airbus X-labs
Taufkirchen, Germany
Michael.m.cooper@airbus.com

Abstract—In recent decades, a growing focus has been on reducing fossil fuel consumption and minimizing CO₂ emissions in the transportation sector. The aerospace industry, which accounted for more than 2% of global carbon emissions in 2021, has taken measures to address this issue. One promising solution to achieve this objective is the development of fully electric aircraft (FEA). In this regard, superconducting technology offers promising advantages, including compactness, lightweight, and higher efficiency to speed up this transition. This work considers a superconducting propulsion system for an electric aircraft. Among the components, the modeling of resistive superconducting fault current limiter (RSFCL) and superconducting DC cable are studied. These models are simulated by MATLAB programming and SIMULINK, and the results are shown. The models analyze their electrical-thermal behavior in a short-circuit and in normal operation conditions. Finally, a SIMULINK model containing the fault limiter and cable is simulated, and the results are presented. As a result, different models are compared and suitable designs are presented for both applications.

Index Terms—Electric Aircraft, Superconducting Fault Current Limiter, Superconducting DC Cable

I. INTRODUCTION

A. Motivation and Background

The focus on combating climate change and decreasing CO₂ emissions has given significant attention to transportation electrification. This includes the swift advancement of electric vehicles in various sectors, such as roads, railways, and shipping, as a direct response to this environmental concern. In 2021, aircraft were accountable for approximately 2.4% of the world's carbon emissions [1]. Considering the potential substantial growth in aircraft production [2], this contribution is projected to increase significantly.

The aerospace industry has set ambitious goals, including the EU Flightpath 2050 plan, which aims to achieve a 75% reduction in carbon emissions [3]. One potential solution that has emerged is the concept of full electric aircraft (FEA), which could offer a viable means to achieve this objective [4]. Superconductors provide benefits in power systems compared to conventional alternatives in terms of their compactness,

lightweight nature, and higher efficiency [5], [6]. At present, various electrical components, including fault current limiters (FCLs), cables, machines, and transformers have already reached a high technology readiness level. As a result, implementing a superconducting powertrain in electric aircraft seems viable and enables the aviation industry to build first demonstrators [4]- [6].

B. Schematic of the Aircraft Powertrain

The proposed powertrain design consists of multiple components, starting with the DC source and extending to the propeller's motor [7]. Situated between these components are DC/DC and DC/AC converters, which enable voltage amplitude variation and conversion. To ensure efficient current transportation to the motor, superconducting DC and AC cables are employed. Moreover, a resistive superconducting fault current limiter (RSFCL) is incorporated into the system to prevent sudden rises in current caused by potential short circuits. The schematic of the proposed powertrain is shown in Fig. 1. For this study, liquid nitrogen (LN₂) at a temperature of 77 K is the cooling medium for the system.

This work focuses on modeling two key components of the powertrain in electric aircraft: the resistive superconducting fault current limiter (RSFCL) and the superconducting DC cable. The electrical-thermal behavior of both components is thoroughly analyzed, and the methodology for simulating their behavior is outlined. The study utilizes MATLAB programming and SIMULINK models to conduct the simulations. The simulation results, which provide insights into the performance and behavior of the RSFCL and superconducting DC cable, are then presented and discussed.

II. STUDY CASE

The simplified study case network consists of a 300 VDC source, a transmission line, and a load, with a fault occurring at the load location. The schematic of this case is provided in Fig. 2. The current flowing in the network in nominal

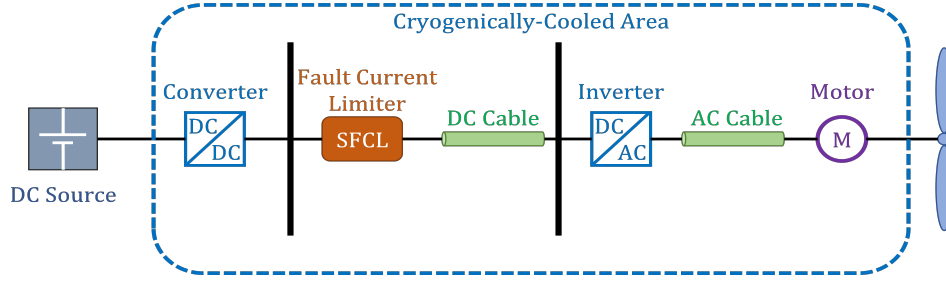


Fig. 1. Schematic of the Electric Aircraft Superconducting Powertrain [7]

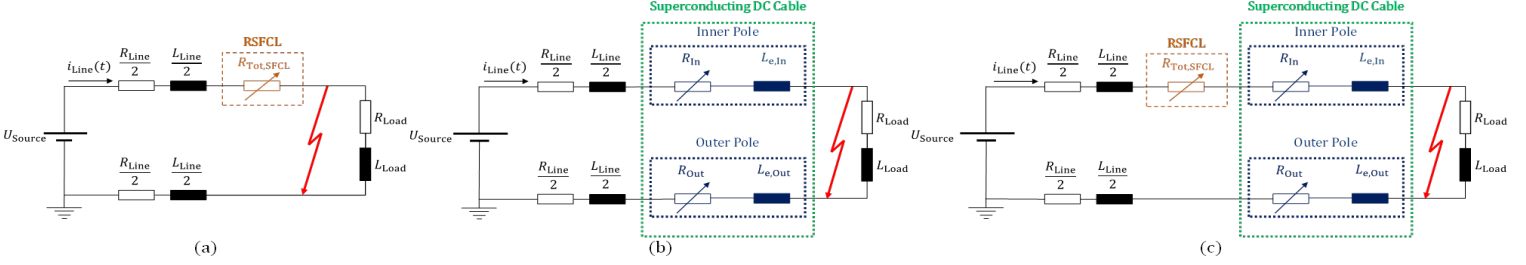


Fig. 2. Schematic of the Study Case Network: (a) with Only RSFCL, (b) with Only Superconducting DC Cable, (c) with Both RSFCL and Cable

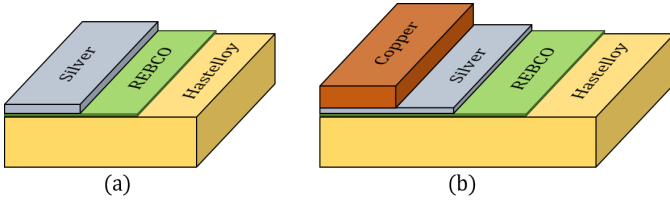


Fig. 3. Structure of the considered HTS tapes for: (a) RSFCL, (b) DC cable

TABLE I
PROPERTIES OF THE CONSIDERED HTS TAPES FOR THE RSFCL AND DC CABLE

Parameter	Specification		Unit
	RSFCL	Cable	
Tape Width	12	4	mm
Tape Length	8.5	50	m
Copper Thickness	-	40	μm
Silver Thickness	4	3	μm
REBCO Thickness	1	2	μm
Hastelloy Thickness	100	75	μm
Tape Total Thickness	105	120	μm
Tape Critical Temperature	92	92	K
Tape Critical Current	550	200	A

conditions is 1.5 kA, and the steady-state short circuit current due to the pole-to-pole fault at the load location is 15 kA. Firstly, a stand-alone model for an RSFCL and a superconducting cable are analyzed as seen in Fig. 2(a) and Fig. 2(b), respectively. Then the combination of both components is investigated (Fig. 2(c)).

III. RESISTIVE SUPERCONDUCTING FAULT CURRENT LIMITER

A. Introduction

Maintaining stability in an electrical network relies on limiting fault current and safeguarding the equipment [8], [9]. Superconducting fault current limiters (SFCLs) offer promising solutions for effectively and rapidly limiting short-circuit currents [8], [10]. These SFCLs have several advantages, including their reliability and effectiveness and their significantly low impedance during normal operation, making them an attractive alternative to conventional current limiting methods [10]. There are various types of fault limiters, including resistive SFCLs, saturated inductive SFCLs, and shielded inductive SFCLs [10]. Among these, resistive SFCLs (R-SFCLs) are the simplest and most well-established solution compared to the other types. The RSFCL is placed in series with other network elements, as depicted in Fig. 2(a). The parameter $R_{\text{Tot,SFCL}}$ denotes the total resistance of the HTS tapes in the RSFCL.

B. Design and Properties

An SFCL is made up of superconducting tapes or wires. This study considers a High Temperature Superconducting (HTS) REBCO tape with a critical temperature of above 90 K and a critical magnetic field of more than 100 T. The HTS tape has three layers: one for REBCO as superconductor, and the other two are silver (Ag) as a stabilizer and Hastelloy (Hy) as a substrate. The structure of the HTS tape can be seen in Fig. 3(a). Additionally, TABLE I provides detailed information about the tape properties, including its electrical-thermal characteristics and geometry specifications. Considering that the nominal current flowing through the SFCL is 1.5 kA, and

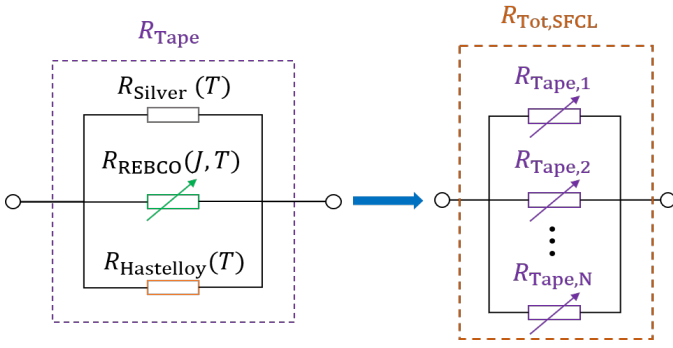


Fig. 4. Electrical Characteristic Illustration of the RSFCL

the critical current of each HTS tape is 550 A, three HTS tapes need to be connected in parallel to carry the nominal current.

C. Modeling

To model the RSFCL, the lumped-parameter method is used. In this model, the electrical and thermal characteristics of the RSFCL are taken into account.

a) *Electrical Characteristic*: The electrical characteristic of an SFCL is primarily related to its resistance. Each tape within the SFCL has its resistance, and the layers within each tape also contribute to the overall resistance. This is depicted in Fig. 4.

The parallel resistance law is applied to calculate the resistance of a single tape R_{Tape} from resistances of tape sub-layers: resistance of the silver layer R_{Silver} , resistance of the REBCO superconductor layer R_{REBCO} , and resistance of the Hastelloy substrate layer $R_{Hastelloy}$. Equation (1) illustrates this relationship.

$$\frac{1}{R_{Tape}} = \frac{1}{R_{Silver}} + \frac{1}{R_{REBCO}} + \frac{1}{R_{Hastelloy}} \quad (1)$$

Furthermore, when multiple tapes are employed in an SFCL (N tapes), assuming they have identical properties, resistances, and temperatures, the total resistance of the SFCL, $R_{Tot,SFCL}$, is obtained by equation (2).

$$R_{Tot,SFCL} = \frac{R_{Tape}}{N} \quad (2)$$

In contrary to the linear (with temperature T) behavior of the silver and Hastelloy layers with temperature [12], the resistance of the REBCO superconductor acts non-linearly. The relationship between electric field E and current density J in the REBCO superconductor follows a power law known as the E-J power law [12], [13]. The resistivity of the superconductor ρ is calculated based on this rule using equation (3).

$$\rho = \frac{E}{J} \quad (3)$$

b) *Thermal Characteristic*: In this work, it is assumed that all tapes in the SFCL have the same temperature, and there is no temperature gradient within the tapes

($T_{Silver}=T_{REBCO}=T_{Hastelloy}=T_{Tape}$). Moreover, The temperature of cooling media (LN_2) remains constant at 77 K ($T_{LN_2} = 77$ K).

The tape temperature T_{Tape} is calculated with following equation:

$$C_{Tape} \cdot \frac{\partial T_{Tape}}{\partial t} = P_{Tape} - P_c \quad (4)$$

with C_{Tape} as the tape heat capacity, P_{Tape} as the power loss in the tapes, and P_c as the cooled (convected) power by cooling fluid.

The power loss in the tapes P_{Tape} can be calculated based on the tape current I_{Tape} and resistance R_{Tape} using equation (5).

$$P_{Tape} = R_{Tape} \cdot I_{Tape}^2 \quad (5)$$

The cooled power P_c is dependent on the heat transfer conditions; in the adiabatic condition, there is no convected power from the tapes to the cooling media ($P_{c,Adiabatic} = 0$), while in the non-adiabatic environment, heat convection occurs between the tapes and the cooling fluid, which reduces the tape temperature. The calculation of P_c in non-adiabatic condition is described in equation (6):

$$P_{c,Non-Adiabatic} = 2h_{c,LN_2} \cdot w_{Tape} \cdot l_{Tape} \cdot \Delta T \quad (6)$$

with h_{c,LN_2} as LN_2 convective heat transfer coefficient, w_{Tape} as tape width, l_{Tape} as tape length, and ΔT as the difference between T_{Tape} and T_{LN_2} . The convective heat transfer coefficient h_{c,LN_2} is calculated like the following equation where the values of α_i can be found in [12]:

$$h_{c,LN_2} = \begin{cases} 2170 & ; \Delta T \leq 3.2 \\ \sum_{i=0}^5 \alpha_i \cdot \Delta T^i & ; 3.2 < \Delta T \leq 28 \\ \frac{3970 + \Delta T}{\Delta T} & ; \Delta T > 28 \end{cases} \quad (7)$$

Initially, the temperature of all tapes is 77 K, and the temperature increase in the tapes ΔT_{Tape} can be calculated based on equation (4) using the following equation, considering the time-step Δt :

$$\Delta T_{Tape} = \Delta t \cdot \left(\frac{R_{Tape} \cdot I_{Tape}^2 - P_c}{C_{Tape}} \right) \quad (8)$$

As seen in this equation, the tape resistance and current play a major role in the calculation of the temperature. Assuming the same properties and resistance for all tapes, the current is evenly distributed among the parallel tapes. The line current in this study case is determined using Kirchhoff's Voltage Law (KVL). Due to the tapes' non-linear resistance caused by the superconductor resistance's non-linearity, an analytical equation cannot be used to calculate the line current. Therefore, a numerical method is required to calculate its value. The implicit method is utilized in this work. Furthermore, since the superconductor can operate in different states depending

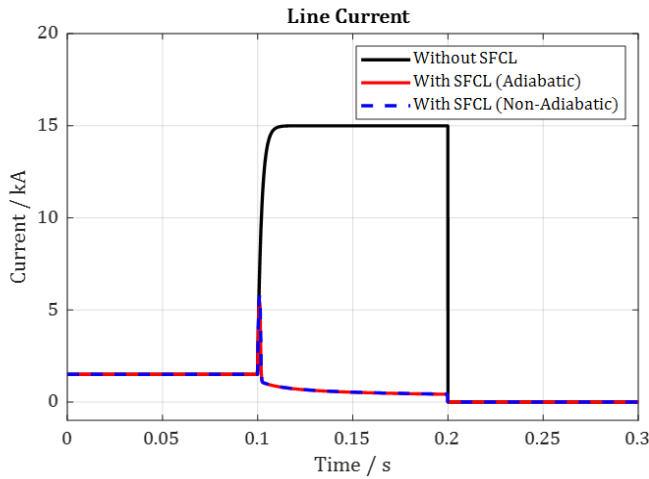


Fig. 5. Line Current Profile with/without Presence of SFCL

on the flowing current, a robust approach to precisely calculate its resistance with a high level of accuracy is needed [12].

D. Simulation Results

The RSFCL is simulated with MATLAB programming, and a SIMULINK model for the study case is developed. Considering the line current, Fig. 5 illustrates the changes in the line current i_{Line} across three scenarios. This figure shows that the RSFCL has successfully limited the fault current to almost 6 kA. The current limitation provided by the SFCL is primarily due to the transition of the superconductor from superconducting state to the normal state. Under nominal conditions, where the resistance of the REBCO superconductor is nearly zero, the SFCL does not impose any losses into the system. Therefore, there is no noticeable difference between the scenario with the SFCL and the scenario without it. Another important observation from this figure is the negligible difference between the RSFCL performance in the adiabatic and non-adiabatic models during the fault.

Furthermore, Fig. 6(a) and Fig. 6(b) present results regarding the variation in the tape temperature, T_{Tape} and tape resistance, R_{Tape} . When a fault occurs, the tape temperature increases significantly, surpassing the critical temperature of the superconductor (quench), causing a remarkable increase in the tape resistance as well. This temperature rise is similar in both the adiabatic and non-adiabatic models. The main difference between these models is observed after fault clearance (100 ms after fault occurrence). In the adiabatic model, where no heat dissipation occurs from the tapes to the coolant, the temperature and resistance remain constant at their peak values ($T_{Tape,Max} = 242$ K, $R_{Tape,Max} = 2.1$ Ω). While, in the non-adiabatic model, the coolant absorbs the generated heat from the tapes, reducing their temperatures, and after around 1.9 seconds, the tape temperature gradually returns to 77 K, enabling it to revert to its superconducting state ($R_{Tape} = 0$ Ω).

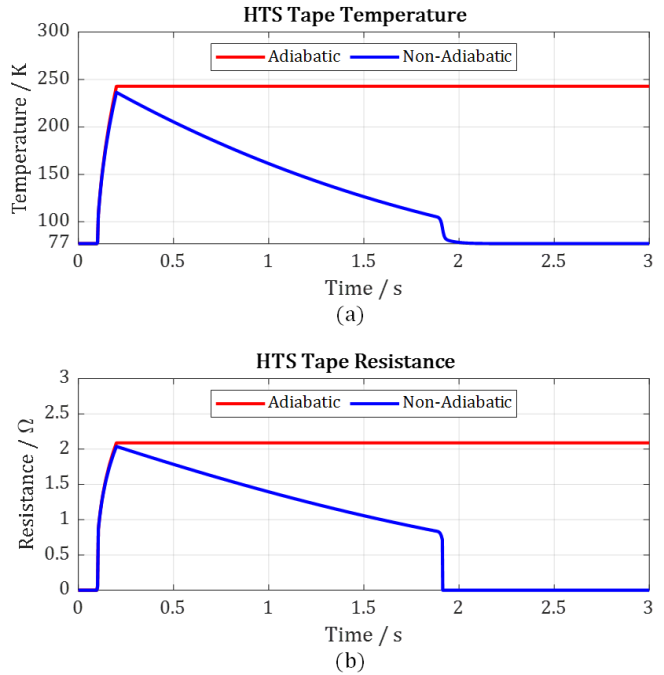


Fig. 6. Tape Temperature and Resistance Profiles in the RSFCL: (a) Tape Temperature, (b) Tape Resistance

IV. SUPERCONDUCTING DC CABLE

A. Introduction

Superconducting cables have been further developed in recent decades [14]– [16]. These cables offer promising advantages such as smaller size, higher current density, lower loss, and higher security compared to conventional rivals [15], [16]. These advantages have been a motivation to further commercialize superconducting cables and use them in existing power systems [14], [15], [17].

B. Design and Properties

A superconducting DC cable can be used in monopolar or bipolar DC systems. In this work, a bipolar DC cable is considered. The structure of this cable is depicted in Fig 7, while the radius of each layer is specified in TABLE I. The superconducting cable comprises several layers starting from the cable's center and extending towards the sheath. These include a core copper layer and a single layer of HTS tapes in the inner pole. Furthermore, a Polypropylene Laminated Paper (PPLP) layer provides insulation between the poles. Another layer consisting of HTS tapes and shield copper is present for the outer pole. Finally, there is a coolant flowing duct within the cryostat. In this work, similar to the RSFCL, LN₂ at 77 K is used to cool the superconductor.

The HTS tape considered for this cable has a similar structure to the tapes considered for the SFCL, with the difference that there is an additional copper sub-layer in the tapes of the cable. The structure of this HTS tape is shown in Fig 3(b), and its properties are described in TABLE I. To make the coaxial DC cable with the geometry as depicted in Fig 7, 8

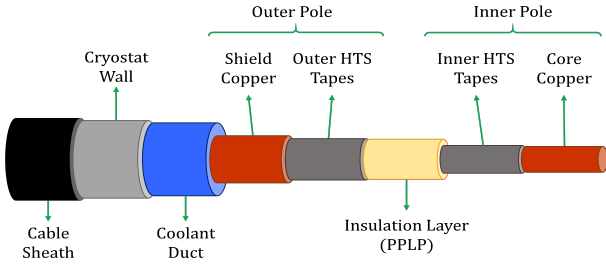


Fig. 7. Structure of the Bipolar Superconducting DC Cable

TABLE II
PHYSICAL GEOMETRY SPECIFICATIONS OF THE BIPOLAR
SUPERCONDUCTING DC CABLE

Parameter	Symbol	Specification	Unit
Core Copper Diameter	d_{Core}	10	mm
Outer Diameter of Inner HTS Tapes	$d_{Tapes,In}$	10	mm
PPLP Outer Diameter	$d_{PPLP,Out}$	15	mm
Outer Diameter of Outer HTS Tapes	$d_{Tapes,Out}$	15	mm
Shield Copper Outer Diameter	$d_{Sh,Out}$	18	mm
Cooling Fluid Outer Diameter	$d_{Fld,Out}$	28	mm
Cable Outer Diameter	$d_{Cable,Out}$	30	mm
Cable Length	l_{Cable}	50	m

and 12 HTS tapes with these specifications are required for the inner and outer poles, respectively. Since the critical current of the tapes is influenced by the magnetic field, it is crucial to determine the maximum applied field on each tape. This calculation shows that the maximum applied magnetic field on an HTS tape within this configuration is approximately 65 mT. The critical current of the tape I_c at this magnetic field and LN₂ temperature (77 K) is approximately 200 A.

C. Modeling

Similar to the RSFCL, a superconducting DC cable has electrical and thermal characteristics.

a) *Electrical Characteristic:* Each conducting layer of the cable, including the HTS tapes, has its own resistance within the cable. The parameters R_{In} and R_{Out} are the total resistances of the inner and outer poles, R_{Core} and R_{Shield} correspond to the resistances of the core copper and shield copper layers, and $R_{Tapes,In}$ and $R_{Tapes,Out}$ are the resistances of the tapes in the inner and outer poles, respectively. The equivalent circuit of the HTS tapes has the same principle as explained for RSFCL in Section III (refer to Fig 4). The resistance of the tapes is calculated based on the resistances of the sub-layers using the parallel resistor law (See equation (1) in Section III). Similarly, the parallel resistance law is applied to calculate each pole's resistance. For example, the inner pole resistance R_{In} is computed using equation (9).

$$\frac{1}{R_{In}} = \frac{1}{R_{Tapes,In}} + \frac{1}{R_{Core}} \quad (9)$$

Unlike the SFCL, each pole of the cable has an inductance that must be taken into consideration. The parameters $L_{e,In}$

and $L_{e,Out}$ denote the effective inductances of the inner and outer poles, respectively (See Fig 2(b)). These inductances incorporate the mutual inductance between the poles [18]. The cable poles are in series; therefore, the total cable resistance R_{Cable} is calculated based on series resistances law from the resistances of the inner and outer poles, and the cable inductance L_{Cable} is calculated with the inductance equation of the coaxial cables given in [18]. Similar to the RSFCL, the network current i_{Line} cannot be computed analytically since the cable resistance is non-linear. Therefore, the same approach in using a numerical method must be applied.

b) *Thermal Characteristic:* To thermally model the cable, the lumped-parameter, adiabatic model is used. In this model, no heat transfer/convection between the layers is considered, and each layer possesses a single temperature (no temperature gradient across the layer): $T_{Tapes,In}$ represent the temperature of the inner tapes, and $T_{Tapes,Out}$ indicate the temperature of the outer tapes. Initially, due to the thermal balance between all the layers, the temperature of all cable layers is set at 77 K, the coolant temperature. To calculate the increase in the temperature of each layer ΔT_{Layer} , the same principle as RSFCL is applied. Thus, it is determined by the power loss in each layer, taking into account the layer resistance R_{Layer} , current I_{Layer} , and heat capacity C_{Layer} . This relationship is depicted in equation (10), considering the time step Δt . The general term 'Layer' in this equation applies to all cable layers.

$$\Delta T_{Tape} = \Delta t \cdot \left(\frac{R_{Layer} \cdot I_{Layer}^2}{C_{Layer}} \right) \quad (10)$$

D. Simulation Results

MATLAB programming is used to simulate the cable, and a corresponding SIMULINK model is developed. Similar to the simulation of the RSFCL, the design of the cable and other components in the network can be customized according to the user's preferences and requirements.

Figure 8 depicts the current variation in the layers of the inner pole, which includes the core copper and sub-layers of the HTS tapes. The black curve represents the line current in the network without the cable, while the blue curve represents the network with the cable. The dark red curve represents the current flowing through the core copper. Within the HTS tapes, the current through the REBCO sub-layer is indicated with a green curve, the copper (Cu) sub-layer with a red curve, the silver (Ag) sub-layer with a dashed gray curve, and the Hastelloy sub-layer (Hy) with a dashed orange curve. This figure demonstrates that the presence of core/shield copper, which has relatively low resistances, does not cause a significant increase in the total resistance of the cable. As a result, the line current is only slightly limited. This can be attributed to the behavior observed after a fault, where the current exceeds the superconductor's critical current I_c . During this transition from the flux creep regime to the flux flow regime, most of the current is diverted towards the core/shield copper due to

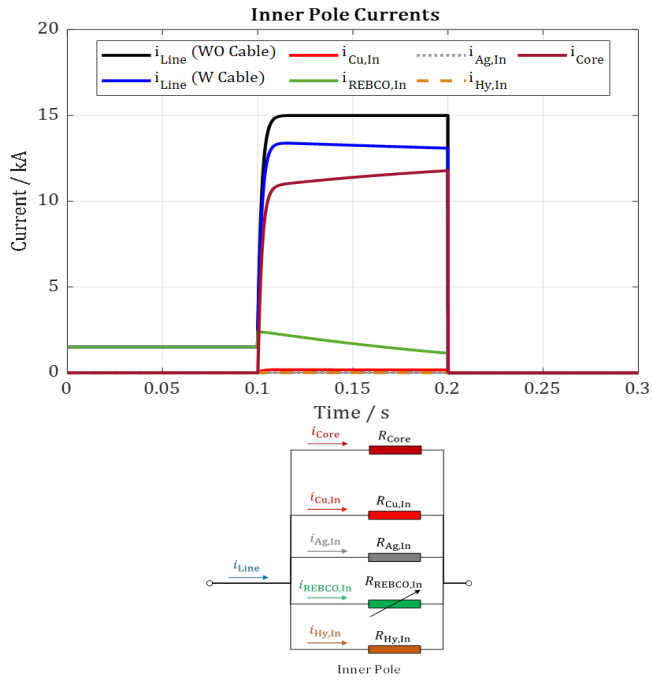


Fig. 8. Line Current Profile alongside the Currents of the Inner Pole Layers

their lower resistances. The relatively higher resistances of the other sub-layers in the HTS tapes result in negligible currents flowing through them. Figure 9(a) and Figure 9(b) illustrate the variation in temperatures and resistances of the HTS tapes, respectively. These results reveal that the current shifts from the tapes to the core/shield copper after the fault occurs. As a result, the temperatures of the tapes do not experience a significant increase and remain below the critical temperature (no quench), ensuring that their resistances only have a slight increase (due to the transition of the REBCO state from flux creep to flux flow). Consequently, the limitation of the fault current is relatively minor. It is important to note that in this particular model, the cable is assumed to be in an adiabatic condition, meaning that the layers are not cooled from liquid nitrogen (LN_2). As a result, after the fault is cleared, the temperatures of the cable layers remain constant.

V. SIMULATION OF THE CABLE EQUIPPED WITH THE FAULT CURRENT LIMITER

In previous sections, the simulation results demonstrated the effectiveness of an RSFCL in limiting fault currents and the efficient current transport capability of a superconducting cable in electric aircraft. However, it was observed that the cable alone could not effectively limit the fault current. As a result, the combination of an RSFCL and a superconducting cable is considered a promising solution to enhance the fault current limitation capability. The schematic of the study case network incorporating both the RSFCL and the cable was shown in Fig. 2(c). Figure. 10 demonstrates the line current obtained from the simulation of the study case under different scenarios. This figure illustrates that with the assistance of the

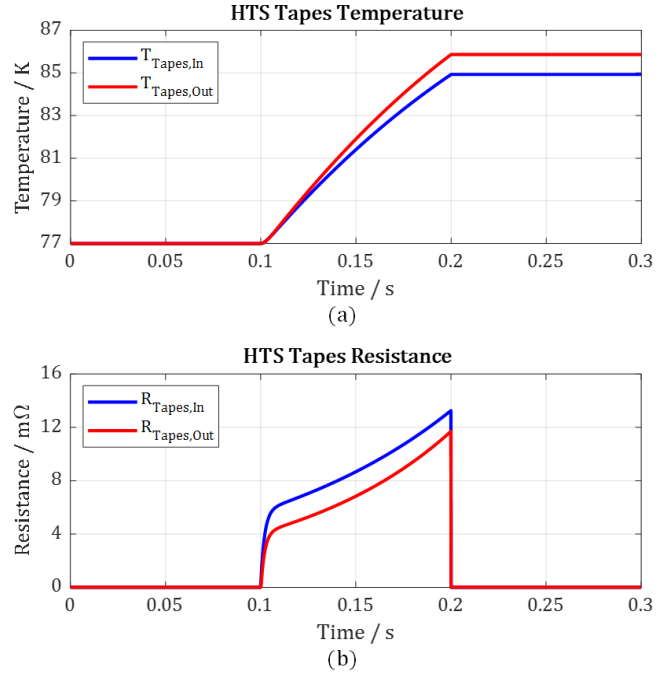


Fig. 9. Tapes Temperature and Resistance Profiles in the Cable: (a) Tapes Temperature, (b) Tapes Resistance

fault limiter (SFCL), the fault current is effectively limited. Moreover, Fig. 11(a) and Fig. 11(b) show the variation of the temperature and resistance of the tapes used in the SFCL and cable. These figures also confirm that with the presence of fault limiter, the temperature and resistance increase in the tapes of cable is relatively negligible, while it is significant for the tapes in the SFCL. Therefore, the SFCL protects the cable from any sudden rise in the temperature.

VI. CONCLUSIONS AND PERSPECTIVE

This study focused on two components of the superconducting powertrain in an electric aircraft as a promising solution for reducing CO_2 emissions: the resistive superconducting fault current limiter (RSFCL) and the DC cable. The behavior of these components was simulated using MATLAB programming. It is seen that the RSFCL limits the fault current effectively without overheating the superconducting tapes. Moreover, contrary to the similar behavior during fault in the adiabatic and non-adiabatic models, the main difference between these conditions lies in the long time (e.g., after fault). In opposite to the adiabatic model, in the non-adiabatic model, the cooling fluid absorbs the heat generated in the tapes leading to the reduction in their temperature and reverting to the superconducting state. In the analysis of the bipolar DC cable, the study revealed similar behavior to the RSFCL, but it was observed that due to the presence of two parallel layers of copper in addition to the HTS tapes, the cable does not effectively limit the fault current. The core and shield copper layers have relatively low resistances, resulting in a low total resistance for the cable poles. Consequently, when a

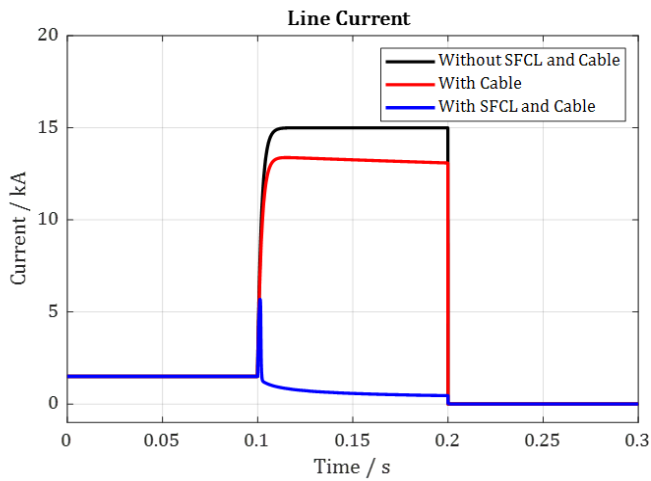


Fig. 10. Line Current Profile highlighting the Effect of SFCL in the Network with Cable

fault occurs, the current tends to flow through these copper-based layers rather than the superconductor sub-layers in the HTS tapes. As a result, the temperature of the HTS tapes experiences an insignificant increase, preventing them from quenching. Therefore, adding an SFCL becomes necessary to restrict the fault current and protect the system effectively. The main perspective of this work is modeling other superconducting components of electric aircraft, with a particular focus on the superconducting motor. Furthermore, more advanced and detailed cable models, including one-dimensional and two-dimensional models, have been developed. The upcoming research work will present these enhanced cable models and provide further insights into the behavior and performance of superconducting cables in electric aircraft and other power systems.

REFERENCES

- [1] T. C. Cano et al., "Future of Electrical Aircraft Energy Power Systems: An Architecture Review," *IEEE Transactions on Transportation Electrification*, vol. 7, no. 3, pp. 1915–1929, Sep. 2021, doi: 10.1109/TTE.2021.3052106.
- [2] "Global Market Forecast, Airbus." <https://www.airbus.com/en/products-services/commercial-aircraft/market/global-market-forecast> (accessed Jun. 22, 2023).
- [3] P. O. of the E. Union, "Flightpath 2050: Europe's vision for aviation: maintaining global leadership and serving society's needs.," Jun. 2011, doi: 10.2777/50266.
- [4] K. Kovalev, J. Nekrasova, N. Ivanov, and S. Zhurzvlev, "Design of All-Superconducting Electrical Motor for Full Electric Aircraft," *Proceedings - ICOECS 2019: 2019 International Conference on Electrotechnical Complexes and Systems*, Oct. 2019, doi: 10.1109/ICOECS46375.2019.8949952.
- [5] C. A. Luongo et al., "Next generation more-electric aircraft: a potential application for hts superconductors," *IEEE Transactions on Applied Superconductivity*, vol. 19, no. 3, pp. 1055–1068, Jun. 2009, doi: 10.1109/TASC.2009.2019021.
- [6] F. Berg, J. Palmer, P. Miller, and G. Dodds, "HTS System and Component Targets for a Distributed Aircraft Propulsion System," *IEEE Transactions on Applied Superconductivity*, vol. 27, no. 4, Jun. 2017, doi: 10.1109/TASC.2017.2652319.
- [7] L. Ybanez et al., "ASCEND: The first step towards cryogenic electric propulsion", doi: 10.1088/1757-899X/1241/1/012034.

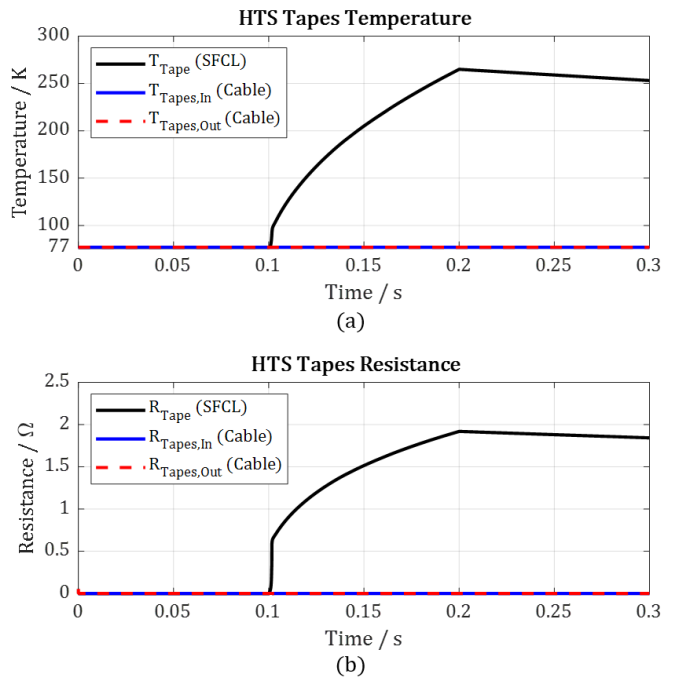


Fig. 11. Tapes Temperature and Resistance Profiles in the SFCL and Cable: (a) Tapes Temperature, (b) Tapes Resistance

- [8] O. Näckel and M. Noe, "Conceptual Design Study of an Air Coil Fault Current Limiter," *IEEE Transactions on Applied Superconductivity*, vol. 23, pp. 5602404–5602404, Apr. 2013.
- [9] K. Yasuda et al., "Research & development of superconducting fault current limiter in Japan," *IEEE Transactions on Applied Superconductivity*, vol. 15, no. 2, pp. 1978–1981, 2005, doi: 10.1109/TASC.2005.849349.
- [10] O. Näckel and M. Noe, "Design and Test of an Air Coil Superconducting Fault Current Limiter Demonstrator," *IEEE Transactions on Applied Superconductivity*, vol. 24, no. 3, pp. 1–5, 2014, doi: 10.1109/TASC.2013.2286294.
- [11] F. Mumford, "Superconducting fault current limiters," *IEE Colloquium on Fault Current Limiters - A Look at Tomorrow*, pp. 6/1–6/7, 1995.
- [12] W. T. B. de Sousa, "Transient Simulations of Superconducting Fault Current Limiters," Ph.D. Dissertation, Federal University of Rio de Janeiro, Brazil, 2015.
- [13] P. E. Sutherland, "Analytical model of superconducting to normal transition of bulk high T_c superconductor BSCCO-2212," *IEEE Transactions on Applied Superconductivity*, vol. 16, pp. 43–48, Mar. 2006.
- [14] D. W. Kim et al., "Development of the 22.9-kV class HTS power cable in LG cable," *IEEE Transactions on Applied Superconductivity*, vol. 15, no. 2 PART II, pp. 1723–1726, Jun. 2005, doi: 10.1109/TASC.2005.849266.
- [15] X. H. Zong, D. Wei, Y. W. Han, T. Tang, Z. Y. Zhang, and Z. G. Yu, "Development of 35kV 2000A CD HTS cable demonstration project," *2015 IEEE International Conference on Applied Superconductivity and Electromagnetic Devices, ASEMD 2015 - Proceedings*, pp. 593–595, Apr. 2016, doi: 10.1109/ASEMD.2015.7453717.
- [16] V. Pothavajhala, L. Graber, C. H. Kim, and S. Pamidi, "Experimental and model based studies on current distribution in superconducting DC Cables," *IEEE Transactions on Applied Superconductivity*, vol. 24, no. 3, 2014, doi: 10.1109/TASC.2013.2282568.
- [17] V. E. Sytnikov et al., "Status of HTS cable link project for St. Petersburg Grid," *IEEE Transactions on Applied Superconductivity*, vol. 25, no. 3, Jun. 2015, doi: 10.1109/TASC.2014.2373814.
- [18] F. W. Grover, *Inductance Calculations*. Dover Phoenix Editions, 2004.